Bangladesh Journal of Physics, Vol. ***28****, Issue 2, pp. 39-50, December 2021*

SPIN-COATED Cu_2NiSnS_4 THIN FILMS: THE IMPACT OF THIOUREA'S MOLAR CONCENTRATION

M. M. RASHID[1*], A. A. NOMAN[1], S. ISLAM[2], F. AHMED[2], M. S. BASHAR[3], M. S. UDDIN[1], A. T. M. K. JAMIL[1] AND S. J. AHMED[1]

[1]*Department of Physics, Dhaka University of Engineering & Technology, Gazipur, Gazipur-1707, Bangladesh*
[2]*Department of Physics, Jahangirnagar University, Savar-1342, Bangladesh*
[3]*Institute of Fuel and Research Development, Dhaka-1205, Bangladesh*

[*]*Corresponding author e-mail: mamun92@duet.ac.bd*

Received on 26.06.2021, Revised received on 14.08.2021, Accepted for publication on 11.11.2021

DOI: https://doi.org/10.3329/bjphy.v28i2.78588

ABSTRACT

Copper-Nickel-Tin-Sulfide, Cu_2NiSnS_4 (CNTS) thin films are deposited on to glass substrates through simple and cost-effective spin coating technique, with the variations in the molar concentration of thiourea (MCT). In this research, $CuCl_2.2H_2O$, $NiCl_2.6H_2O$, $SnCl_2.2H_2O$ and $SC(NH_2)_2$ are utilized as the sources of copper, nickel, tin, and sulfur ions, respectively. The influence of MCT on the structural, morphological, and optical properties of the CNTS thin films have been investigated. The XRD results reveal that all CNTS thin films exhibit a cubic crystalline structure and a preferential orientation along the (111) plane. The mean crystallite size for the intense peak (111) is found to enhance from 7.24 to 10.81 nm with MCT. Conversely, the dislocation density and microstrain are found to decrease from 1.91×10^{-2} to 0.86×10^{-2} $\mathrm{lines/nm^2}$ and 4.8×10^{-3} to 3.2×10^{-3}, respectively. The density and surface roughness of the films are also found to increase with MCT. The absorption coefficient (on the order of $\approx 10^5\ \mathrm{cm^{-1}}$), refractive index, extinction coefficient, dielectric constant, and optical conductivity all increased, while the percentage transmittance and optical band gap decreased with MCT. These outcomes suggest that CNTS thin film could a promising material for the use as an absorbing layer in photovoltaic applications and optoelectronic devices.

Key-words: *CNTS, MCT, Thin films, Cubic structure*

1. INTRODUCTION

As the world's population continues to grow quickly, the daily need for energy is also increasing. The primary energy sources, known as fossil fuels, mostly supply this need. Moreover, burning fossil fuels depletes CO, CO_2, SO_2, NO_2, and other harmful elements, which leads to adulteration. Therefore, it is imperative to identify and utilize environmentally sustainable, renewable energy sources in lieu of conventional energy resources. Today, there are many well-known sources of renewable energy. Among these, solar energy considers as the most prevalent, sustainable, and productive energy source available to humans [1].

Silicon substrate technologies, both crystalline and polycrystalline, account for more than 70% of the current photovoltaic (PV) market. However, to absorb a greater percentage of incident solar energy, these technologies require a thin layer of absorbing material. Furthermore, perfect crystals are required to produce high-efficiency solar modules, which results in expensive PV devices. To address the world's growing energy needs, modern PV advancements have increasingly focused on thin film (TF) PV technologies as a replacement for traditional PV technologies.

The direct optical band gap (E_g) materials CIGS, CdTe, and CIS constitute the foundation of these types of TF PV technologies. However, the manufacturing of PV devices focusing on these absorber layers is limited and narrowed due to the toxicity of Se and Cd as well as the attainability concerns of Te and In. As an alternative, researchers have been greatly intrigued by the present focus on absorber chemicals that are abundant on Earth, environmentally benign, inexpensive, and non-toxic [1]. Because of these challenges, the quaternary semiconductor Cu_2ZnSnS_4 (CZTS) has gained attention as a suitable absorber layer in thin films for photovoltaic solar cells over the past few years. CZTS thin films are abundant in the earth, less expensive, and less poisonous. There are more potential flaws in CZTS thin films depending on the conditions of fabrication, stoichiometry variations, and, most importantly, anti-sites Cu_{Zn}, Sn_{Zn} and Zn_{Sn}. These faults adversely affect the efficiency of CZTS solar cells [2, 3]. It appears that there are two primary axes into which the studies of semiconductor absorbers can be divided: The replacement of Zn^{2+} by other elements with similar valence electrons, such as $Fe^{2+,}$ $Co^{2\,+}$, and Ni^{2+}, has tempted serious motives for the advancement of CZTS TF in solar cells for PV implementation. The optimal low-cost semiconductor absorber layers Cu_2FeSnS_4 (CFTS), Cu_2CoSnS_4 (CCTS), and Cu_2NiSnS_4 (CNTS) are expanded by this kind of study [4–8]. These quaternaries can be applied in a variety of ways, including photovoltaics, sensors, thermo-electricity, spintronics, photolysis, and batteries.

CNTS is currently an adjustable compound for PV solar cell implementations due to its high absorption capacity ($\approx 10^5$ cm^{-1}), p-type semiconducting behavior, and appropriate E_g range. Additionally, it lacks costly and rare chemical reagents like gallium (Ga) and indium (In), and the materials that make up this kind of film are inexpensive, abundant on Earth, and environmentally benign. Lu *et al.* [9] reported the maximum conversion efficiency of CNTS solar cells, which is comparable to the highest efficiency of the CZTS absorbance substances. Previously, researchers have studied p-type semiconducting CNTS nanoparticles using various physical and chemical deposition techniques, such as spin coating [5, 9], facile solvothermal [10,11], novel hydrothermal route [12], electrodeposition [13,14], spray pyrolysis [15], molecular ink [16], chemical bath deposition [17], hot injection [18], among others. They used $CuCl_2$, $NiCl_2$, $SnCl_2$, and $SC(NH_2)_2$ as sources of Cu, Ni, Sn, and S, respectively. Most researchers have used excess MCT to deposit the films, thereby violating the stoichiometric ratio (2:1:1:4). They have used this excess MCT arbitrarily, such as, 8 M, 10 M, or 12 M, respectively. This is because, during the synthesis process, sulfur tends to volatilize easily as gases. However, no optimization research is currently available that provides specific conditions for the deposition of CNTS films to achieve almost a stoichiometric composition and compensate for this loss. Therefore, the main purpose of this study is to identify the optimized MCT for preparing CNTS thin films to achieve improved structural, morphological, and optical properties. To this end, we prepared the films by varying the MCT using a simple spin-coating technique. Our results indicate that to synthesis high-quality CNTS thin films, 12 M thiourea should be used as the sulfur source.

2. EXPERIMENTAL DETAILS

In this experiment, we deposited CNTS thin films on glass substrates using the spin coating technique. First, the glass substrates and beakers were cleaned for 5 minutes with de-ionized (DI) water, followed by 5 minutes with ethanol, and then 5 minutes with acetone. The cleaned substrates and beakers were then dried at 60 ºC using a horizontal drying oven (Model: 202-OA, China). After weighting the appropriate amounts of $CuCl_2.2H_2O$, $NiCl_2\cdot 6H_2O$, $SnCl_2\cdot 2H_2O$, and $SC(NH_2)_2$ (sources of Cu, Ni, Sn, and S) using a balance, all the reagents were added to a beaker and dissolved in 2-methoxyethanol, which acts as the solvent. A few drops of Mono-ethanolamine (MEA) were also added as a stabilizer. The prepared solution was then stirred for 60 minutes at 50 ºC using a magnetic stirrer (Model: 78-1 Magnetic Heating Stirrer, China) to ensure dissolution of the reagents. The solution was then deposited on to the substrates using a vacuum spin coater (Model: VTC-100PA, Germany) at 2000 rpm for 1 minute. After the first coating, the samples were pre-heated at 120 ºC for 10 minutes using the aforementioned oven to evaporate the solvents. To obtain the appropriate film thickness, this coating process was carried out for eight times. Finally, for re-crystallization, the samples were annealed at 340 ºC for 30 minutes using a furnace (Model: KLS 10/12, Germany).

The structural properties of the fabricated CNTS thin films were characterized using an XRD machine (Model: BRUKER D8 XRD, Germany), morphological properties were examined using an analytical electron microscope (Model: JEOL JSM-6490LA, Japan), and optical properties were analyzed using ultraviolet-visible spectroscopy (Model: UH4150 spectrophotometer, Japan).

3. RESULTS AND DISCUSSION

3.1 Structural analysis

Figure 1 illustrates the XRD patterns of spin-coated CNTS thin films deposited with the variation in the MCT. Four major peaks are observed, corresponding to the planes (111), (200), (220), and (311) of the CNTS phase (JCPDS card no. 00-026-0552). All the samples exhibit a cubic crystalline structure belonging to the F-43m space group. The intensity of the XRD peaks increases with increasing MCT, indicating an improvement in crystalline quality. This is because an increase in MCT provides sufficient sulfur to fully form the crystal lattice, thereby enhancing the film's crystallinity and structural integrity. This may also be due to removing of the defects with the increment of MCT [19].

The structural parameters like interplaner spacing (*d*), lattice parameter (*a*), the average crystallite size (*D*), dislocation density (δ), and microstrain (ε) are calculated using the following relation for the intense peak (111) [19].

$$d_{hkl} = \frac{n\lambda}{2Sin\theta} \quad \text{.........................(1)}$$

$$a = d\sqrt{h^2 + k^2 + l^2} \quad \text{...............(2)}$$

$$D = \frac{K_S\lambda}{\beta Cos\theta} \quad \text{..........................(3)}$$

$$\delta = \frac{1}{D^2} \quad \text{.............................(4)}$$

$$\varepsilon = \frac{\beta\ Cos\theta}{4} \quad \text{..........................(5)}$$

Here, λ, K_S, β and θ are the X-ray source wavelength (0.15406 nm), Scherrer’s constant (0.9), FWHM in radians and peak position in radians, respectively.

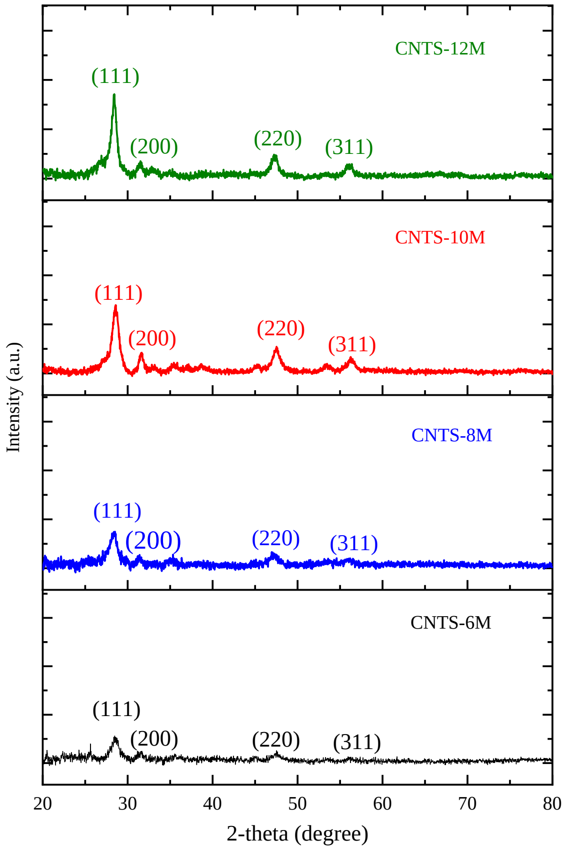

Fig. 1. X-ray diffraction pattern of different CNTS films

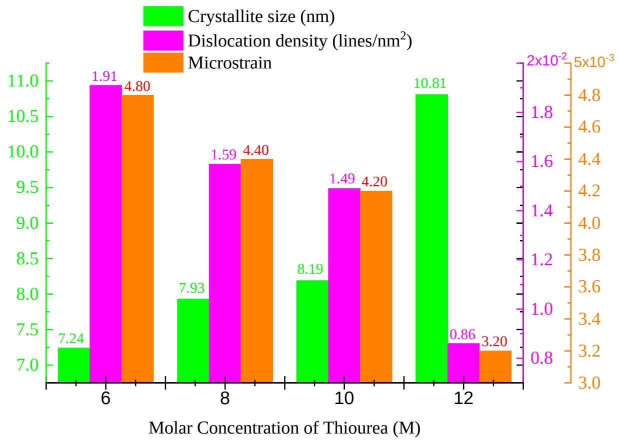

Fig. 2. Structural parameters as a function of MCT

Figure 2 shows that the average crystallite size (*D*) increases significantly from 7.24 to 10.81 nm with MCT. This increase is attributed to the enhanced availability of sulfur, which promotes better crystallization, reduces defects, and facilitates the growth of larger crystallites in the thin films. Additionally, both microstrain and dislocation density are found to decrease with the increment of MCT. This effect may be linked to the increasing relative intensity of the diffraction peaks with MCT. Elsewhere, for all CNTS thin film, the interplanar spacing (*d*) and lattice constant (*a*) are found nearly constant, at 3.131 Å and 5.424 Å, respectively. This outcome aligns with the findings reported in the literature [20].

3.2 Morphological analysis

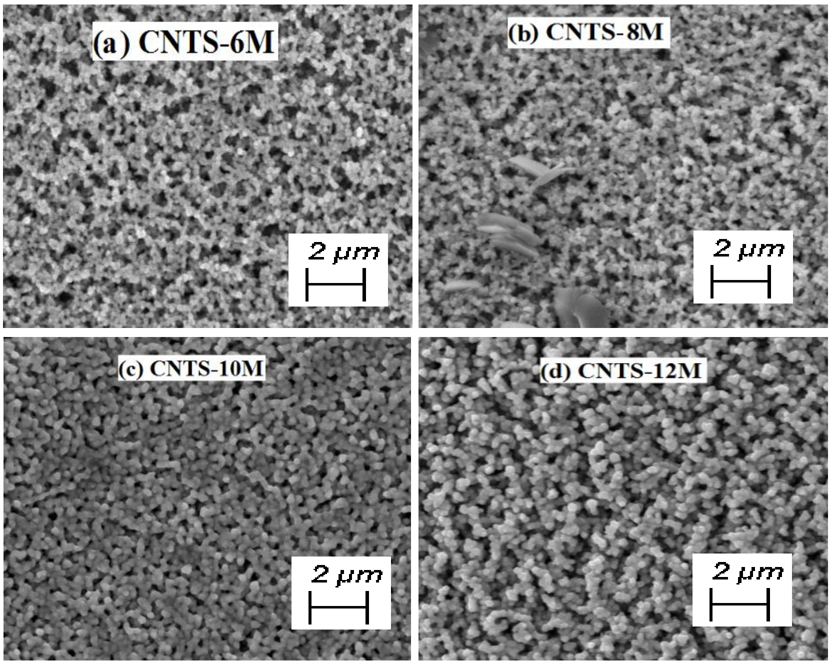

Fig. 3 SEM micrographs of the CNTS films at various MCT, taken a magnification of × 5.00 K.

The SEM images of CNTS thin films at different MCT values, captured at a magnifications of × 5.00 K, are displayed in Fig. 3 (a–d). All the films exhibit a compact surface, surrounded by numerous uniformly sized, spherical grains that are densely packed together. In the CNTS-8M thin film, a few larger spots are also visible, but these are actually the result of the smaller grains accumulating. Additionally, as we observed that the crystallite size increases with MCT, it can be stated that the density and surface roughness of the films also increase with the sulfur ion source. This observation also aligns well with the findings of an earlier study [21]. However, it is widely recognized that maximizing photoelectrochemical performance requires a photoelectrode to have a high surface area and effective contact with electrolyte interfaces [22]. Therefore, as surface roughness and film density increase with MCT, it can be declared that the photocurrent density and efficiency of CNTS thin films are influenced by MCT.

3.3 Optical analysis

The variation of absorbance (A) with wavelength (λ) in the range of 250 – 1200 nm for the deposited CNTS films, is depicted in Fig. 4. From the figure, it is observed that absorbance increases sharply in the ultraviolet (UV) region, reaching its peak value. Afterward, absorbance gradually decreases in the UV, visible (VIS), and near-infrared (NIR) regions, eventually becoming nearly flat in the NIR region. Similar trends have been reported by former researchers [10–14, 23]. It is also noted that A rises with MCT, which could be attributed to the enhanced crystallinity induced by the higher MCT.

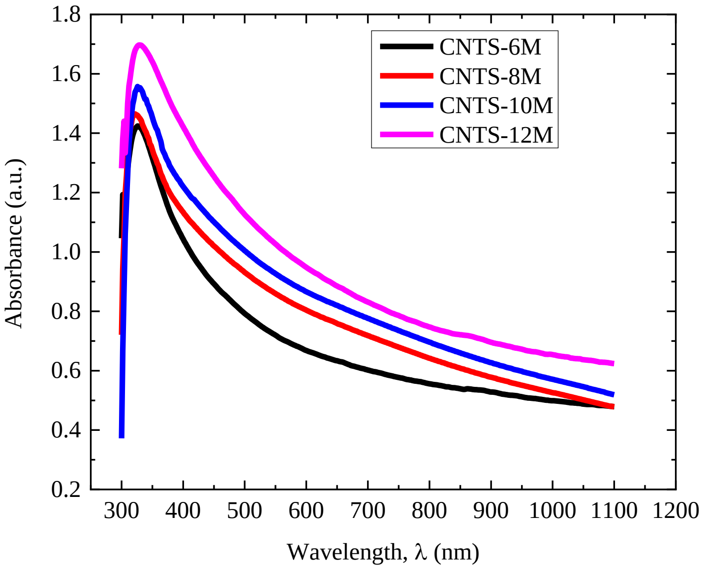

Fig. 4 Absorbance variation with wavelength

The %transmittance, *T (%)*, is calculated using the following relation [7] and is shown in Fig. 5,

$$T(\%) = 10^{(2-A)} \ldots\ldots\ldots\ldots\ldots\ldots\ldots\ldots(6)$$

From Fig. 5, it is observed that as the wavelength increases, *T (%)* rapidly drops in the UV region, reaching a minimum value, and then increases linearly from the UV region to the VIS region, followed by a further increase from the VIS region to the NIR region. Ziti *et al.* [2] previously observed a similar trend. Additionally, it is noted that as MCT increases, *T (%)* decreases. This is due to the increased density of the films with higher MCT, as denser films tend to absorb more light, reducing transmittance. The %transmittance is notably low in the UV region, suggesting that no transmission happens at lower wavelengths due to complete absorption of the incident light.

The CNTS thin film's optical absorption coefficient (α) is computed using the equation mentioned below [6].

$$\alpha = \frac{2.303\,A}{t} \ldots\ldots\ldots\ldots\ldots\ldots\ldots\ldots\ldots\ldots \text{(7)}$$

Here, t refers to the thickness of the film.

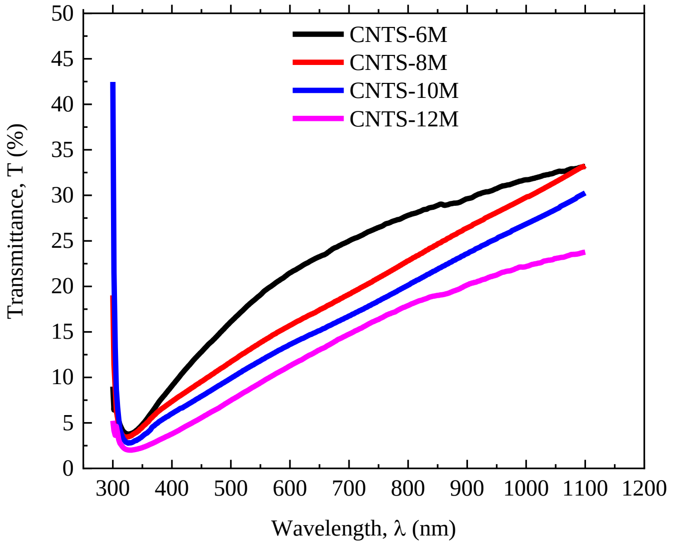

Fig. 5. %Transmittance variation with wavelength

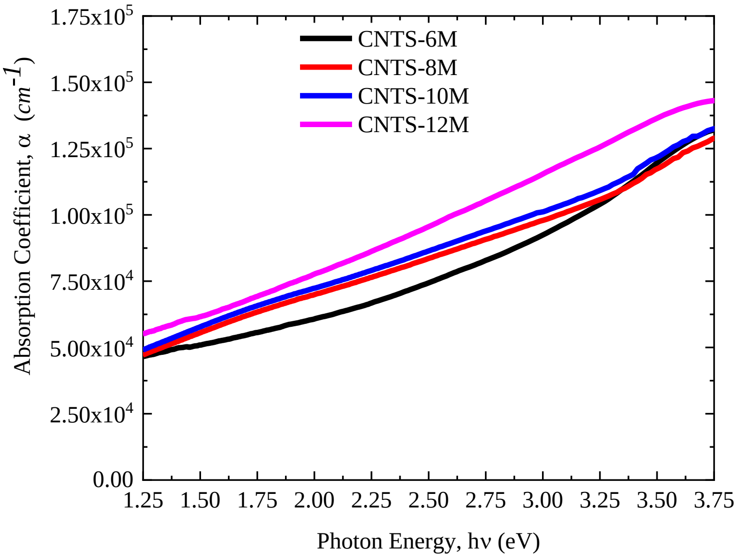

Fig. 6. Absorption coefficient variation with photon energy

Figure 6 illustrates how the photon energy of CNTS thin films affects the absorption coefficient. It has been noted that the absorption coefficient rises with photon energy and is lowest at lower energies. Additionally, it is observed that α increases with MCT, and in the visible region, α is in the range of ≈ 10^5. This occurs due to the increased absorption with MCT. The increase in α with MCT suggests a greater possibility of direct transitions. Therefore, it can be said that the possibility of a direct transition in CNTS thin films increases with the MCT of the film.

The optical direct gaps (E_g) of CNTS films are obtained by using Tauc formula [19],

$$\alpha h\nu = A_0(h\nu - E_g)^n \ldots\ldots\ldots\ldots\ldots\ldots\ldots\ldots \text{(8)}$$

Here, A_0 and n represent the energy dependent constant and index that depends on the type of optical transition induced by the photon absorption, respectively.

The $(\alpha h\nu)^2$ versus photon energy ($h\nu$) plot for the different CNTS films is shown in Fig. 7. The estimated band gap energies for the CNTS thin films are as follows: 2.12 eV for CNTS-6M, 2.08 eV for CNTS-8M, 2.06 eV for CNTS-10M, and 1.90 eV for CNTS-12M. It is seen that the value of E_g decreases with the increase in MCT. This may be due to the increase in crystallite size with MCT, as larger crystallizes bring the electron-hole pair closer together, thereby lowering E_g. Similar trend was also reported by Ahmed *et al.* [24].

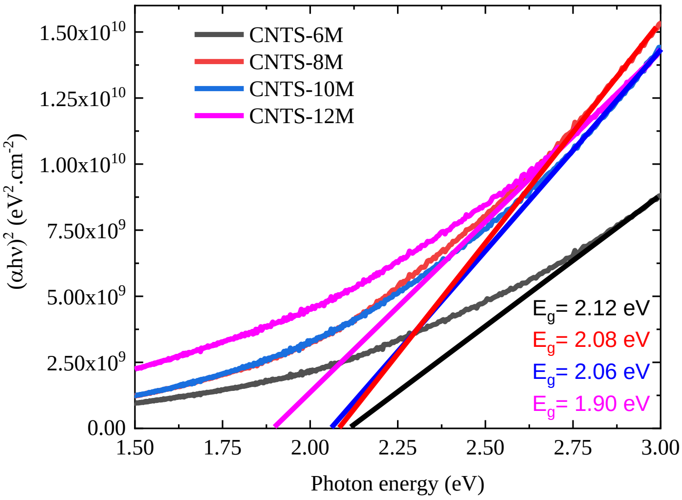

Fig. 7 $(\alpha h\nu)^2$ variation with photon energy

The formula for calculating the refractive index (n) is [2, 25],

$$n = \frac{1+R}{1-R} + \sqrt{\frac{4R}{(1-R)^2} - {k_E}^2} \ldots\ldots\ldots\ldots\ldots\ldots\ldots\ldots\ldots \text{(9)}$$

Here, R denotes the reflectance and k_E represents the extinction coefficient.

Figure 8 represents the variation of the refractive index with respect to wavelength. For each film, it is observed that the refractive index increases quickly in the UV region, reaches a peak value, then decreases from the UV region to the VIS region, from the VIS region to the NIR region, and finally becomes nearly flat in the NIR region. This behavior demonstrates standard dispersion protocol. Other research groups have also noticed a similar trend [2, 25]. Additionally, it is noted that the refractive index increases with the increment of MCT. Since it is well known that light speed decreases as material density increases, which in turn increases the refractive index, this may be due to both the increase in density and crystallite size with MCT of the films. Deokate *et al.* [23] reported a similar outcome. Since high crystallinity is accredited by greater values of refractive index, hence it can be terminated that crystallinity depends on MCT or the sulfur ion source of the film.

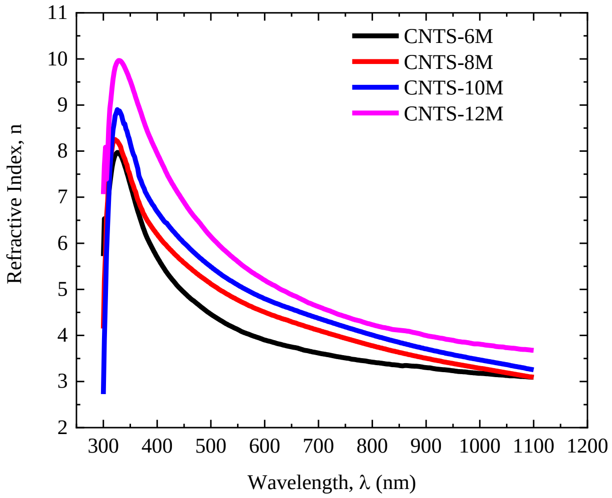

Fig. 8 Refractive index variation with wavelength

The following equation is used to obtain the optical extinction coefficient (k_E), which is shown as a function of wavelength with the variation of MCT in Fig. 9 [2].

$$k_E = \frac{\alpha\lambda}{4\pi} \ldots\ldots\ldots\ldots\ldots\ldots\ldots\ldots\ldots\ldots\ldots (10)$$

It is observed that k_E increases rapidly in the UV region, reaches its maximum value,
then declines to a certain level within that region before gradually increasing in the NIR region. Additionally, it is noted that the extinction coefficients are extremely low and consistent with the findings of earlier research [2, 26]. It is also observed that k_E increases with MCT. This behavior may be attributed to the increase in α with MCT [2].

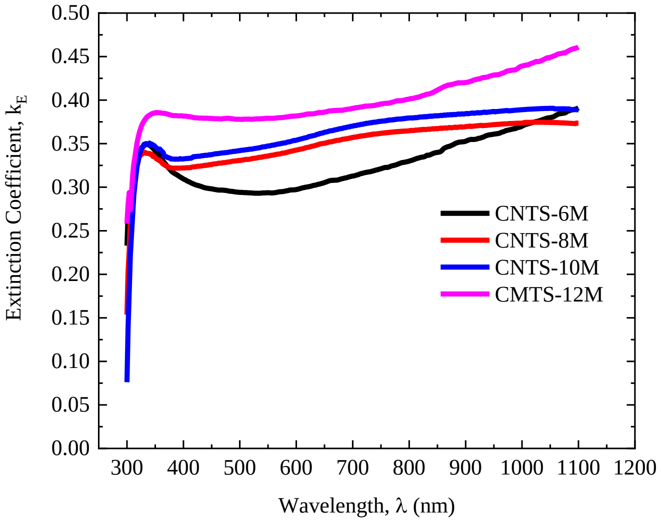

Fig. 9 Extinction coefficient variation with wavelength

The real (ε_r) and imaginary (ε_i) dielectric constants are calculated by utilizing the equations [23, 27],

$$\varepsilon_r = n^2 - {k_E}^2 \ldots\ldots\ldots\ldots(11)$$

$$\text{and } \varepsilon_i = 2nk_E \ldots\ldots\ldots\ldots(12)$$

Figure 10 (a & b) represents the real and imaginary dielectric constants as functions of wavelength. It is observed that both ε_r and ε_i increase quickly in the UV region, reaching their maximum values, and then sharply decrease from the UV to VIS region.

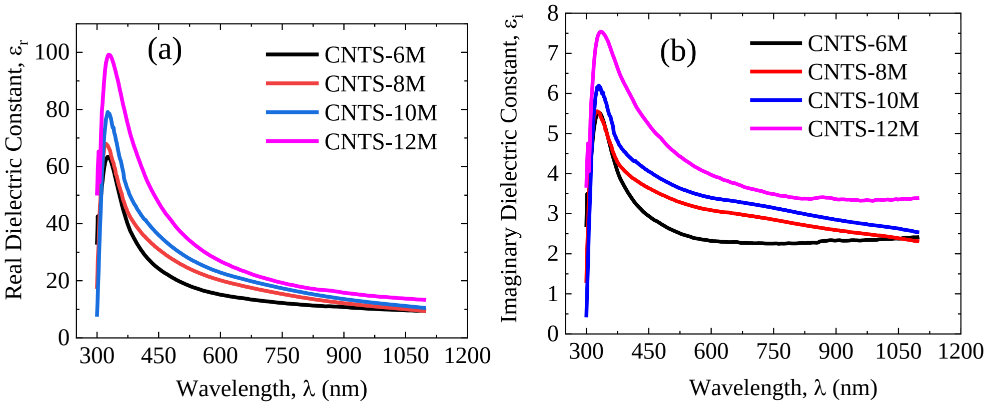

Fig. 10 (a) Real and (b) imaginary dielectric constants variation with wavelength

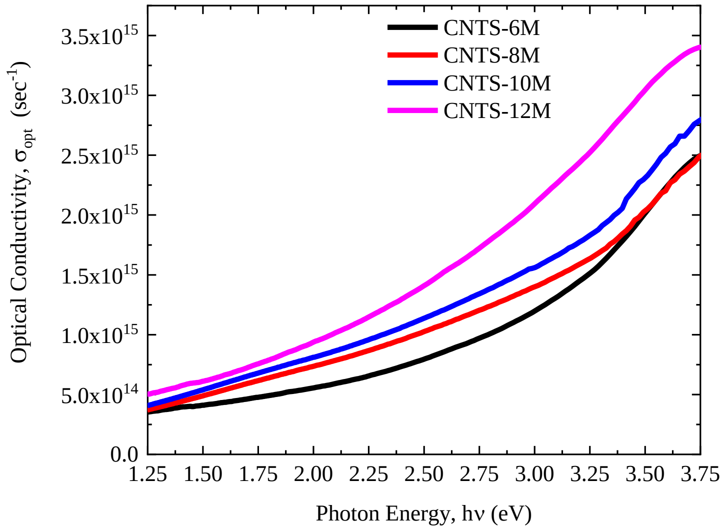

Fig. 11. Optical conductivity variation with photon energy

They eventually become almost perpetual in the NIR region, decreasing slowly from the VIS to the NIR region. Additionally, it is noted that $\varepsilon_r > \varepsilon_i$. These findings are consistent with previous research [2]. Furthermore, both ε_r and ε_i are observed to increase with increasing MCT. This behavior can be attributed to the increase in crystallite size and the reduction in band gap with higher MCT.

The optical conductivity (σ_{opt}) is obtained using the following equation [23, 25] and is depicted in Fig. 11,

$$\sigma_{opt} = \frac{\alpha n c}{4\pi} \text{……………………..(13)}$$

Here, *n* and *c* refer to the refractive index and the speed of light, respectively.

It is observed that with increasing photon energy, σ_{opt} increases slowly from NIR to VIS region and then rises rapidly from the VIS to the UV region. Additionally, σ_{opt} is observed to increase with MCT. This could be associated to the enhanced absorption coefficient and refractive index, as well as the decreasing trend in %transmittance with MCT. It is well known that the motion of photo-excited electrons in thin films governs the progression of σ_{opt}. As the photon energy rises, the speed of electrons intensifies [28], leading to an increase in σ_{opt} for CNTS films. Therefore, it can be concluded that MCT significantly influences the photo-response behavior of CNTS thin films, as evidenced by the increase in σ_{opt} with MCT.

4. CONCLUSIONS

In summary, this study demonstrates the feasibility of synthesizing Cu_2NiSnS_4 (CNTS) thin films on glass substrates using the spin coating technique. The impact of thiourea at varying molar concentrations on the properties of CNTS thin films is thoroughly investigated. All CNTS films display a cubic structure with a dominant orientation along the (111). The crystallite sizes of the CNTS samples range from 7.24 to 10.81 nm. SEM images reveal consistent, spherically-shaped grains, and it is noted that the density and surface roughness of the films rise with MCT. The calculated band gap values range from 2.12 – 1.90 eV, while the absorption coefficient in the visible region is approximately on the order of $\approx 10^5$. Based on the analysis of structural, morphological and optical properties, it can be concluded that the CNTS-12M thin film shows the most promise as an absorber layer for solar cell applications compared to the other CNTS thin films.

REFERENCES

[1] M. P. Suryawanshi, S. M. Bhosale, J. H. Kim, G. L. Agawane, P. S. Patil, S. W. Shin and A. V. Moholkar, Mater. Tech.: Adv. Perf. Mater. **28** (2013) 98.

[2] A. Ziti, A. Belafhaili, B. Hartiti, S. Fadili, H. Labrim, M. Tahri, A. Ridah and P. Thevenin, J. Mater. Sci.: Mater Elec. **32** (2021) 16726.

[3] W. Wang, Y. Zhu, M.T. Winkler, T.K. Todorov, T. Gokmen, O. Gunawan, and D.B. Mitzi, Adv. Energy Mater. **4** (2014) 1301465.

[4] A.M. Alanazi, A. Salhi, F. Alam, A.G. Thomas, P.O. Brien, M. Missous and D.J. Lewis, RSC Adv. **9** (2019) 24146.

[5] A. Ghosh, R. Thangavel, A. Biswas and G. Udayabhanu, RSC Adv. **6** (2016) 96025.

[6] K. Sun, J. Huang, F. Liu, H. Sun, J. Li, X. Cui, Y. Zhamg, A. Wang, J. Cong, Z. Fang, M.A. Green, C. Yan, Y. Lai and X. Hao, J. Mater. Chem. A **7** (2019) 27289.

[7] Y.H. Khattak, S. Ullah, F. Biag, S. Beg, B.M. Soucase and H. Ullah, JNO 13 (2018) 1096.

[8] S. Harinipriya, H. Cassian and V. Sudha, J. Mater. Res. Technol. 15 (2021)3558.

[9] S. Lu, F. Li, H. Yang, S. Chen, Y. Wang, Y. Liu, G. Yang and X. Zhang, Sci. Rep. 8 (2018) 8714.

[10] T.X. Wang, H.R. Liu, H. Li, Y.G. Li and S.X. Chen, Mater. Lett. **124** (2014) 148.

[11] L. Shi, R. Zheng and L. Yanan, ChemPlusChem **80** (2015) 1533.

[12] S. Sarkar, B. Das, G.C. Das, P.R. Midya and K.K. Chattopadhyay, Mater. Lett. **152** (2015) 155.

[13] C. Hui-Ju, F. S. Wen and S. C. Feng, Mater. Lett. **166** (2016) 215.

[14] C.L. Yang, M. Lin, W.C. Liu, L. Li, S.L. Wu, X.S. Wu, Y.H. Chen and F.M. Zhang, Mater. Lett. **166** (2016) 01.

[15] S. Dridi and M. Abaab, Mater. Lett. **204** (2017) 61.
[16] A. Jariwala, S. Patel, T.K. Chaudhuri, V. Kheraj, A. Toshniwal and A. Ray, Mater. Lett. **215** (2018) 118.
[17] N. Bitri, F. Chaabouni, S. Dridi and M. Abaab, Mater. Lett. **213** (2018) 31.
[18] S. Rondiya, Y. Jadhav, N. Wadnerkar, S. Haram, S. Jadkar M. Kabir, Chem. Mater. **29 (2017)** 3133.
[19] S. Dridi, S. Mahjoubi, N. Bitri and F. Chaabouni, J. Mater. Sci.: Mater. Electron. **31** (2020) 7193.
[20] W. Schafer and R. Nitsche, Mat. Res. Bull. **9** (1974) 645.
[21] A. Chihi, B. Bessais and M. F. Boujmil, J. Mater. Sci.: Mater. Electron. **30** (2019) 3338.
[22] M.A. Mansoor, V. McKee, M. Misran, K.G.U. Wijayantha, T.A.N. Peiris, Z. Arifin, N.M. Huang and M. Mazhar, Sol. Energy Mater. Sol. Cells **137** (2015) 258.
[23] R. J. Deokate, S. C. Bulakhe and R. S. Kate, J. Mater. Sci.: Mater. Electron. **30** (2019) 3530.
[24] M. A. Ahmed, N. A. Bakr and A. A. Kamil, CHL **16** (2019) 231.
[25] S.S. Fouad, P. Sharma, M.S. El-Bana and I.M. El Radaf, J. Alloys Compd. **757** (2021) 124.
[26] A. Ziti, A. Belafhaili, B. Hartiti, M. Tahri, H. Labrim, A. Ridah, S. Fadili and P. Thevenin, IOP Conf. Series: Mater. Sci. Engg. **948** (2020) 012025.
[27] M. A. Abed, N. A. Bakr and J. Al-Zanganawee, CHL **17** (2020) 179.
[28] R. Nasrin, H. Kabir, H. Akter and A.H. Bhuiyan, Results in Physics **19** (2020) 103357.